Influence of the Precursor Powder on the Processing Window and Current-Carrying Property of Bi-2212 Wires

Zhenbao Li[1] · Guoqing Liu[1] · Kai Yao[1] · Gaofeng Jiao[1] · Xiaoyan Xu[1] · Qingbin Hao[1] · Lihua Jin[1] · Chengshan Li[1]

Abstract

Four batches of Bi-2212 precursor powders prepared by both the co-precipitation method (CP) and the spray pyrolysis technology (SP) with two compositions (Bi:Sr:Ca:Cu = 2.17:1.94:0.89:2.00, 2.07:1.94:0.89:2.00) were obtained. The feature of the powder was firstly characterized. The faster phase evolution and lower melting temperature range (ΔT) of the precursor powder prepared by SP proved that Bi-2212 powder can be obtained by SP with both a higher preparation efficiency and better composition homogeneity. Then the current-carrying property and microstructure of these wires made from these powders were analyzed comprehensively. The property of the wires was proved to be influenced by the feature of these precursor powders a lot. Wires made by the precursor powder with the better composition homogeneity and higher phase purity were confirmed to hold a larger processing window (T_p). In addition, the decrease of the planar size of Bi-2212 crystals was discovered to improve both the machining homogeneity and texture of the wire. What's more, both the better composition homogeneity of the precursor powder and the larger width of Bi-2212 crystals were found to improve both the interior texture and connectivity of Bi-2212 filaments. For the first time, the article provided quite specific directions to improve the quality of the precursor powder so as to both broaden T_p and enhance the current-carrying property of Bi-2212 wires.

Keywords The spray pyrolysis technology · The composition homogeneity · The processing window · The texture · The connectivity

1 Introduction

$Bi_2Sr_2CaCu_2O_x$ (Bi-2212) superconducting round wire has very high critical current density (J_c) at a low temperature under a high magnetic field [1]. The isotropic round form entails Bi-2212 wires to be twisted directly to make Rutherford cables or cable-in-conduit conductors (CICC) [2–7]. In addition, compared with the other two commercial high-temperature superconductors, that is $Re_1Ba_2Cu_3O_x$ (ReBCO)-coated conductors and $Bi_2Sr_2Ca_2Cu_3O_x$ (Bi-2223) superconducting tapes [8, 9], the alternating current loss of Bi-2212 wires was the lowest [10]. All the above advantages make Bi-2212 wires the most promising superconducting materials to be used in future high-field magnets, such as the high-resolution NMR used in 23T [3] and the high-energy particle accelerator magnets designed to be used in 15–20 T [10, 11].

However, the high-field magnets always need plenty of Bi-2212 wires to reach the required magnetic field, which brought huge challenges to Bi-2212 wires. As we all know, Bi-2212 wires need to be sintered to form the superconducting phase so as to carry a large current. However, the processing window (T_p) of Bi-2212 wires which can hold both a high and stable J_c was quite small in the present stage [12, 13]. Both the large temperature fluctuations in the furnace and the mass heat transfer in Bi-2212 wires itself might both decrease the current-carrying property of Bi-2212 wires and cause severe inhomogeneity distribution of the magnetic field. The small T_p will both bring quite high requirements on the furnace manufacturing technology and lead to the poor performance or even severe damages of the huge magnets, which will definitely increase the cost performance of Bi-2212 wires and limit its engineering applications. Therefore, both broadening T_p and improving J_c for Bi-2212 wires were urgent and necessary to accelerate its practical applications.

However, articles and reports related to T_p of Bi-2212 wires were quite limited [14–16] and methods to broaden it seemed to be less. T.M. Shen et al. had studied the influence

✉ Zhenbao Li
  lizb151206@163.com

1 Superconducting Materials Research Center, Northwest Institute for Nonferrous Metal Research (NIN), Xi'an 710016, China

of both the wire diameter and filament size on T_p of Bi-2212 wires [14]. They mainly found that 1.20-mm and 1.00-mm wires had a larger T_p and 0.8-mm wires had a smaller T_p. The smaller T_p of 0.8-mm wire was mainly ascribed to their severe filaments' coupling. What's more, though two batches of powders with exactly the same preparation method and the same composition were discovered to have different T_p, there was no more detailed discussion about this phenomenon.

Moreover, J_c of Bi2212 wires was studied quite extensively and deeply for a long time. By using the overpressure heat treatment (OPHT) process to decrease the pores in filaments, J_c of Bi-2212 wires was increased by ~7 times compared with that without OPHT [1]. And in 2019, D.C. Larbalestire et al. recorded the highest J_c of Bi-2212 wires by using the precursor powder made by nGimat [17], in which the highest J_c was mainly ascribed to the improved connectivity [17] and the much higher texture of Bi-2212 filaments [18]. As for why the precursor powder made by nGimat entails Bi-2212 wires the highest J_c or how the highest J_c was related to the feature of the precursor powder made by nGimat was not disclosed until now. This makes it difficult to improve J_c of Bi-2212 wires further and will impede the engineering application of Bi-2212 wires to a large extent.

In this article, influence of the precursor powder on both T_p and J_c of Bi-2212 wires was studied comprehensively. Four batches of Bi-2212 precursor powders prepared by two methods with two different compositions were prepared. The feature of the powders was firstly characterized in detail. Then, both T_p and J_c of wires made from these powders were compared and connected closely to the feature of the precursor powders. Finally, the specific methods and directions for both broadening T_p and improving J_c of Bi-2212 wires were provided especially from the aspect of the precursor powder.

2 Experimental Details

2.1 Sample Preparation

Bi-2212 precursor powders with a composition of Bi:Sr:Ca:Cu = 2.17:1.94:0.89:2.00 were synthesized both by the co-precipitation (CP) method and the spray pyrolysis technology (SP), which were marked as CP-Bi2.17 and SP-Bi2.17 respectively. In addition, two batches of Bi-2212 precursor powder with the same composition of Bi:Sr:Ca:Cu = 2.07:1.94:0.89:2.00 were further prepared by SP, which were marked as SP-Bi2.07–1 and SP-Bi2.07–2 respectively. During the two processes, solutions with the designed elemental compositions were all firstly prepared by mixing Bi_2O_3, $SrCO_3$, $CaCO_3$, and Cu with HNO_3. Then, in the CP process, the corresponding nitrate solution was mixed with the oxalic acid precipitant to get the original precipitate. The precipitate was firstly pyrolyzed under 500 °C for 8 h. Then, the pyrolyzed powder was heated and grounded mechanically at 740 °C, 800 °C, 820 °C, 850 °C, and 865 °C successively to obtain the precursor powder. And in the SP process, the corresponding nitrate solution was directly sprayed into a furnace chamber set at 800 °C to get the green powder. The green powder was then heated and grounded manually at 820 °C, 850 °C, and 865 °C successively to obtain the precursor powder. All the sintering process for these powders was undergone in air.

Based on the above four powders, four wires with the same architecture of $(18 + 1) \times 37$ were all prepared using the powder-in-tube (PIT) method and machined to the diameter (d) of 1.00 mm. The three tubes used and the whole machining process were all kept exactly the same for these wires. The loading density was also kept as same as possible around 2.30 ± 0.10 g/cm^3 for the four wires. Details of these lines' mark and their loading density are all listed in Table 1. Then these wires were sintered in a tube furnace (OTF-1200X, Hefei Kejing Material Technology Co. Ltd, USA and China) according to the sintering procedure showed in Fig. 1. Only the maximum temperature (T_{max}) was varied from 882 to 892 °C. The temperature accuracy of the tube furnace can be controlled in ± 1 °C in a temperature range from 850 to 900 °C. Finally, all the sintered wires were annealed under 0.1 MPa Ar with 99.9% purity at 500 °C for 2 h.

2.2 Sample Characterization

The inductively coupled plasma-mass spectrometer (ICP, Nexion 300X, PerkinElmer, America) was firstly used to confirm the practical composition of the precursor powder. Carbon–sulfur analyzer (C-S-600, Leco, USA) and Hydrogen analyzer (RH-600, Leco, USA) were used respectively to check the carbon and hydrogen content in the precursor powder. The powders heated under some specific temperatures were conducted under X-ray diffraction (XRD, Ultima IV, Japan) with Cu K_α source to obtain their phase composition. And the microstructure of the precursor powders was firstly observed under SEM (JSM-6700F, Japan Electronics Co. Ltd and Oxford Instruments, Japan and UK). In addition,

Table 1 The basic information for the four wires prepared in this article

Line mark	Precursor powder used	Loading density (g/cm^3)
W-CP-Bi2.17	CP-Bi2.17	2.29
W-SP-Bi2.17	SP-Bi2.17	2.41
W-SP-Bi2.07–1	SP-Bi2.07–1	2.23
W-SP-Bi2.07–2	SP-Bi2.07–2	2.20

Fig. 1 The schematic sintering procedure for Bi-2212 wires
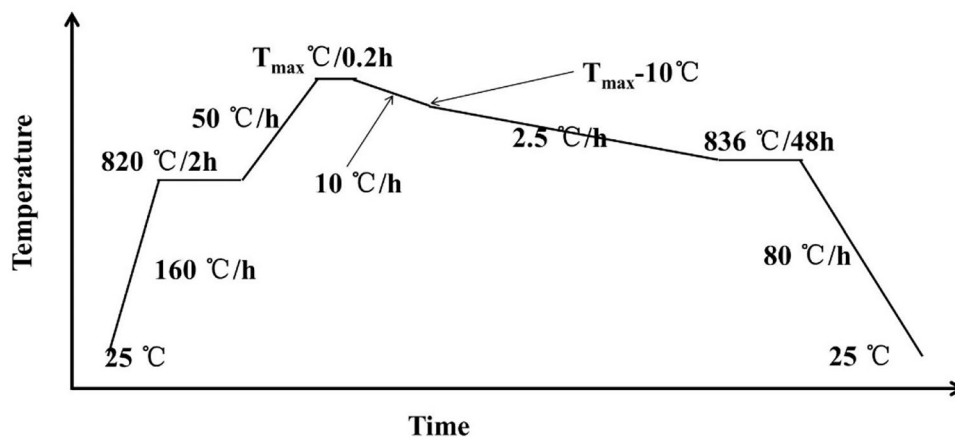
the precursor powders compacted under 10 MPa for 60 s was watched carefully both under SEM and back scattered electron (BSE) pattern at the same place to confirm the existence of the second phase. What's more, the thermogravimetric (TG) and differential scanning calorimetry (DSC, NETZSCH STA 449 F3, Germany) curves for the precursor powders were obtained under O_2 with a heating rate of 10 °C/min from room temperature (RT) until 1000 °C. The melting temperature range (ΔT) for these powders was then determined by referencing the national standard of GB/T 1425–1996.

For both the macrostructure and microstructure observations in these wires, both the machined wires and annealed wires were firstly mounted in the bakelite powder and polished with SiC grinding paper until the grit size of 5–7 μm. Mirror-polished wires were finally obtained by further polishing the above wires on the silk clothes with nano-sized Al_2O_3 solutions as the polishing agent. Then images of the transverse cross-sections for both the machined wires and annealed wires were taken under a light microscope. The filling factor (f), the average diameter (D_a), and the average roundness (R_a) of the superconducting filaments were statistically analyzed by utilization of the image processing software based on the transverse cross-sections of the machined wires. Roundness (R) for every single superconducting filament was defined according to the following equation:

$$R = P^2/(4 * \pi * A) \tag{1}$$

in which, P is the perimeter of a single superconducting filament, and A is the area of the superconducting filament. Then R_a was averaged from all the superconducting filaments in the wire. In addition, the images taken under the light microscopy for the annealed wires were firstly used to check the coupling state of the filaments. Moreover, the annealed wires polished both on the transverse and longitudinal cross-sections were observed under both SEM and BSE pattern to check their detailed microstructure and the second phases.

Besides, the annealed wires were also dealt with the following procedure to check both the texture and connectivity of the filaments on their transverse cross-section. The annealed wires were inserted into small round holes which were drilled into one side of a high-purity graphite cylinder. The diameter of the holes was ~ 1.3 mm and the depth ~ 5–7 mm. The length of these wires was kept the same with the depth of the holes. Then paraffins were melted into the holes by heating and solidified at room temperature so as to fix the wires in the hole. These workpieces mounted with Bi-2212 wires were then polished under the same procedure described above for the wires mounted in the bakelite powder. The wires were then taken out by volatilizing paraffins without damaging the polished surfaces as carefully as possible. Clean and isolated wires with a mirror-polished surface were finally obtained by ultrasonic cleaning in acetone. To check the texture and microstructure of the wires in detail, the above wires were finally sintered under 0.1 MPa oxygen at 800 °C for 1 h and then observed under BSE pattern.

What's more, the annealed wires polished both on the transverse and longitudinal cross-sections were detected under micro-area XRD (D8 Discover, Bruker) with Co source to acquire their phase composition. The selected spot size for the micro-area XRD test was 0.5 mm, which was located around the center of each wire both on the transverse and longitudinal cross-sections. According to the micro-area XRD result, the texture quality for both Bi-2212 phase and Ag on the transverse and longitudinal cross-sections was then evaluated. The texture quality for Bi-2212 phase on the transverse and longitudinal cross-sections was denoted as T_{CS} and T_{LS}, which was coarsely evaluated by Eqs. (2) and (3) respectively. The texture quality of Ag matrix (T_{Ag}) was evaluated by Eq. (4). Then the content of both $Bi_2Sr_2CuO_x$ (Bi-2201) ($M_{Bi-2201}$) phase and $Sr_aCa_{1-a}Cu_bO_x$ (AEC) phase (M_{AEC}) was also evaluated by the corresponding peak intensity ratio according to Eqs. (5) and (6).

$$T_{CS} = \frac{\sum I_{(0k0)}}{\sum I_{Bi-2212}} \times 100\% \qquad (2)$$

$$T_{LS} = \frac{\sum I_{(00l)}}{\sum I_{Bi-2212}} \times 100\% \qquad (3)$$

$$T_{Ag} = \frac{I_{(111)} + I_{(222)}}{\sum I_{Ag}} \times 100\% \qquad (4)$$

$$M_{Bi2201} = \frac{\sum I_{Bi2201}}{\sum I_{Bi-2212} + \sum I_{Bi2201} + \sum I_{AEC}} \times 100\% \qquad (5)$$

$$M_{AEC} = \frac{\sum I_{AEC}}{\sum I_{Bi-2212} + \sum I_{Bi2201} + \sum I_{AEC}} \times 100\% \qquad (6)$$

in which $I_{(0k0)}$ represents for the (0k0) peak intensity of Bi-2212 on the transverse cross-section, $I_{(00l)}$ the (00 l) peak intensity of Bi-2212 on the longitudinal cross-section, $\sum I_{Bi2212}$ the total peak intensity of Bi-2212, $I_{(111)}$ the (111) peak intensity of Ag, $I_{(222)}$ the (222) peak intensity of Ag, $\sum I_{Ag}$ the total peak intensity of Ag, $\sum I_{Bi2201}$ the total peak intensity of Bi2201, and $\sum I_{AEC}$ the total peak intensity of AEC. Moreover, all the above data was calculated again by the peak area, in which the corresponding peak intensity was all replaced by the corresponding peak area. To distinguish the value obtained from the peak intensity and the peak area, the corresponding parameter was added by the suffix of PI and PA respectively.

The critical currents (I_c) for all the annealed wires sintered at different T_{max} were tested at 77 K under self-field based on the DC four-probe transport method with the criterion of 1 µV/cm and the voltage tap distance of ~ 1 cm. I_c for each wire was tested and averaged from two samples considering I_c might fluctuate along the length of the wire. The engineering current density (J_e) was then obtained according to $J_e = 4I_c/\pi d^2$. Then, the largest J_e ($J_{e\text{-}max}$) was obtained for each wire sintered under different T_{max}. T_p was defined as the temperature range in which 90%* $J_{e\text{-}max}$ of the wire could still be sustained. Finally, J_c for each wire was calculated according to $J_c = J_{e\text{-}max}/f$.

3 Results and Discussion

3.1 The Feature of the Precursor Powder

Firstly, ICP and the impurity content of both C and H for the four powders are provided in Table 2. It can be found that the practical composition was basically consistent with the designed composition. Only quite small fluctuations of some elements were a little deviated from the designed value, which was in the range of the detection accuracy of ICP. As for the reason of the deviation for these elements, it needs to be studied further in the future. The total contents of C and H are kept basically the same with each other, which indicated that the impurity gas was not likely to be a main factor affecting J_c in the later discussion.

Figure 2 showed XRD patterns for the four sets of powders pyrolyzed at specific temperatures described in Sect. 2.1, from which the phase evolution for each powder can be discovered. For CP-Bi2.17, it can be found the chemical reactions were still undergone for powders sintered below 820 °C. And until 820 °C, the Bi-2212 phase was the only phase found in all the four powders except SP-Bi2.17. The phase evolution and the related reactions to form Bi-2212 phase in detail can be referenced from Liu's article [19]. Though Bi-2201 was a common medium phase participating in the formation of Bi-2212, the existence of Bi-2201 in SP-Bi2.17 sintered at 865 °C indicated that there were extra Bi-2201 in SP-Bi2.17. Considering both the real time taken and the phase evolution route for powders synthesized by CP and SP, it is found SP had a simpler route and higher rate of Bi-2212 phase formation compared with CP. What's more, with temperature increasing from 820 to 865 °C, the full width at half maximum (FWHM) corresponding to most of the peaks basically showed a decrease trend, which indicated the size of Bi-2212 crystal increased. It is easy to be understood from the aspect of the growth kinetics for Bi-2212 crystals with the temperature increasing.

Figure 3 presented the variation of FWHM corresponding to the crystal plane of (002), (006), (008), (0010), (0012), and (020) respectively for the four precursor powders. It is found that FWHM varied in a same trend for the abovementioned (00 l) except (020). According to the flake feature of Bi-2212 powder, FWHM of (00 l) can be used to evaluate the average planar size of Bi-2212 crystals ($S_{in\text{-}plane}$), and

Table 2 ICP, C, and H content for the four precursor powders

Powder	Designed ICP	Practical ICP	C (ppm)	H (ppm)
CP-Bi2.17	$Bi_{2.17}Sr_{1.94}Ca_{0.89}Cu_{2.00}O_{8+x}$	$Bi_{2.17}Sr_{1.95}Ca_{0.90}Cu_{1.99}O_{8+x}$	160	180
SP-Bi2.17	$Bi_{2.17}Sr_{1.94}Ca_{0.89}Cu_{2.00}O_{8+x}$	$Bi_{2.17}Sr_{1.97}Ca_{0.90}Cu_{2.05}O_{8+x}$	170	140
SP-Bi2.07–1	$Bi_{2.07}Sr_{1.94}Ca_{0.89}Cu_{2.00}O_{8+x}$	$Bi_{2.07}Sr_{1.99}Ca_{0.89}Cu_{2.01}O_{8+x}$	190	160
SP-Bi2.07–2	$Bi_{2.07}Sr_{1.94}Ca_{0.89}Cu_{2.00}O_{8+x}$	$Bi_{2.07}Sr_{1.93}Ca_{0.83}Cu_{2.00}O_{8+x}$	190	150

(a)

(b)
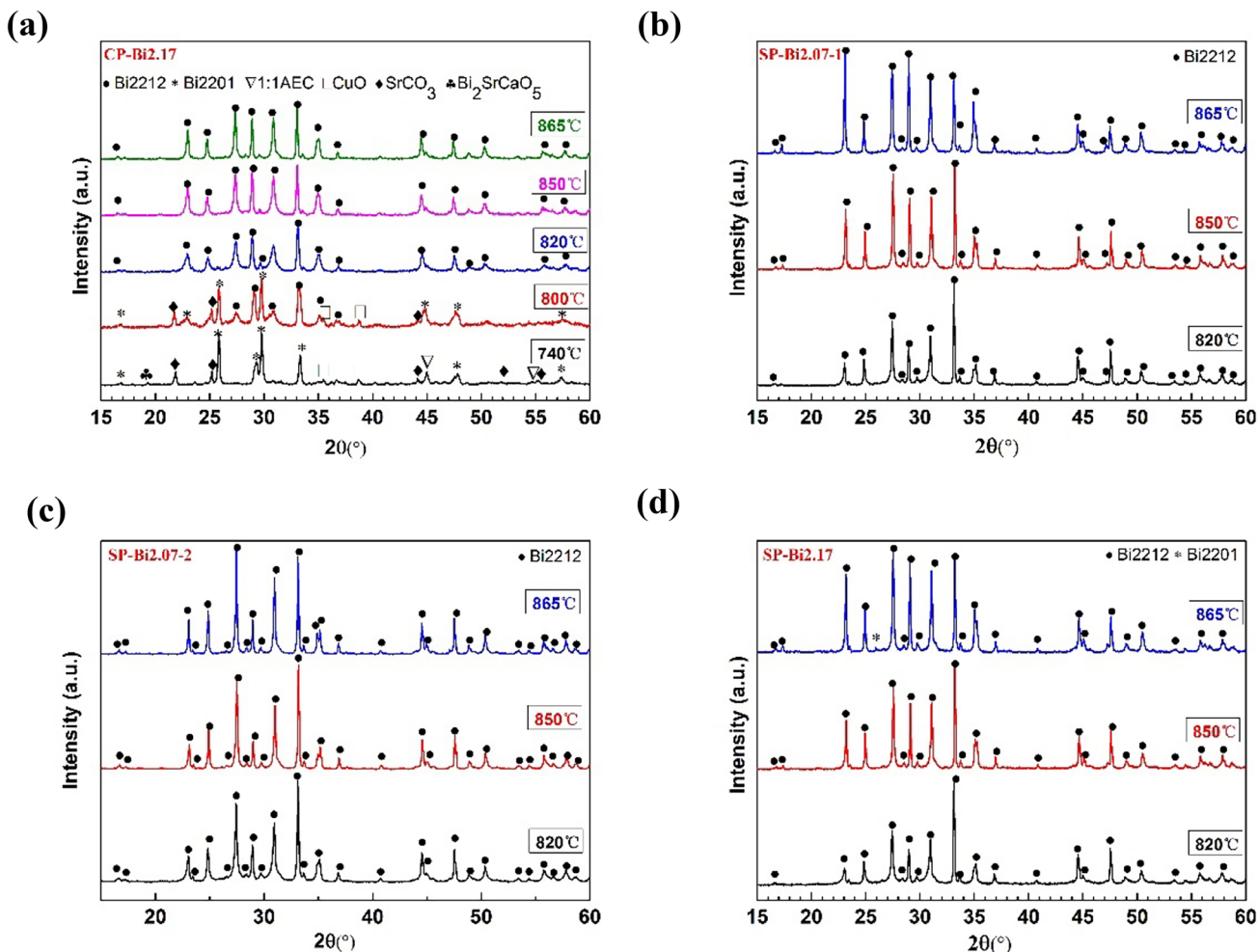

(c)

(d)

Fig. 2 XRD patterns for the four sets of powders pyrolyzed at specific temperatures

FWHM of (020) can be used to evaluate the thickness of Bi-2212 crystals ($S_{\text{in-thickness}}$). A higher FWHM value corresponds to a smaller crystal size often. Therefore, it is
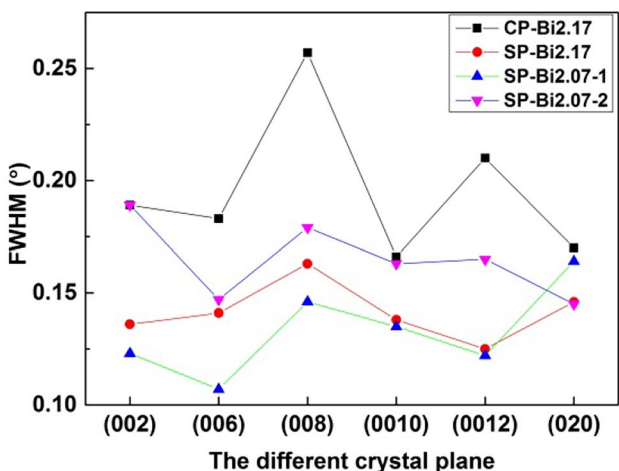

Fig. 3 The variation of FWHM corresponding to (002), (006), (008), (0010), (0012), and (020) respectively for the four precursor powders

deduced that $S_{\text{in-plane}}$ of these powders varied as follows: CP-Bi2.17 < SP-Bi2.07–2 < SP-Bi2.17 < SP-Bi2.07–1; and $S_{\text{in-thickness}}$ varied as follows: CP-Bi2.17 < SP-Bi2.07–1 < SP-Bi2.17 ≤ SP-Bi2.07–2 respectively. And the practical crystal size will be confirmed further by SEM later.

TG and DSC curves for the four precursor powders are showed in Fig. 4a. Figure 4b is the magnification of the DSC curves in Fig. 4a around the melting temperature. ΔT value for the powders is marked in Fig. 4b. From TG curves, it can be found that there are mainly two mass loss stages and the total mass loss varied from 1.32 to 1.68% among these powders. The first mass loss was slow and happened mainly below ~ 880 °C, which was mainly caused by the volatilization of the impurity gas absorbed on the surfaces of the precursor powders. And the second mass loss was quite fast and happened mainly around the melting point of these precursor powders at ~ 890 °C, which indicated the decomposition of the powders. ΔT was 28.5 °C, 21.5 °C, 16.5 °C, and 16.5 °C for CP-Bi2.17, SP-Bi2.17, SP-Bi2.07–1, and SP-Bi2.07–2 respectively. ΔT was discovered to have a close
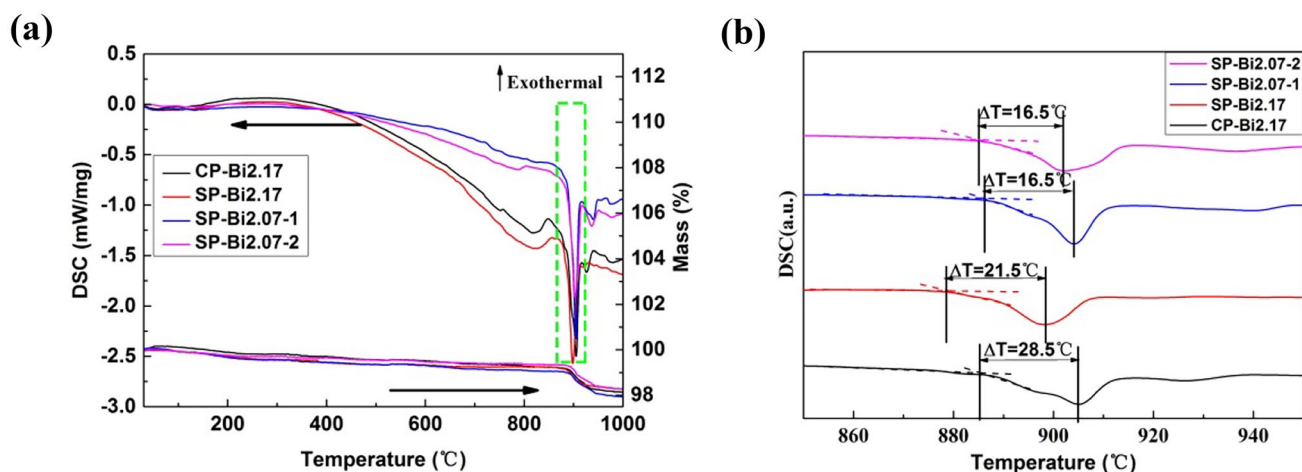
(a)

(b)

Fig. 4 **a** TG-DSC curves. **b** ΔT value for the four precursor powders

relationship with the composition homogeneity of the precursor powders [16, 20]. And a lower ΔT means the better composition homogeneity. It is then deduced that the composition homogeneity of CP-Bi2.17 was worst. Though there was a small content of Bi-2201 in SP-Bi2.17, its ΔT was still smaller than that of CP-Bi2.17. Combing with both the process of the phase evolution and the color homogeneity in BSE showed later for powders obtained by CP and SP, it is speculated that SP had an advantage of synthesizing the precursor powder with a higher composition homogeneity and a higher preparation efficiency. What's more, the composition homogeneity of SP-Bi2.17 was worse than that of SP-Bi2.07–1 and SP-Bi2.07–2, which might be mainly ascribed to the existence of Bi-2201 in its precursor powder. ΔT for SP-Bi2.07–1 and SP-Bi2.07–2 was the same and smallest among the precursor powders, which indicated their best composition homogeneity. However, it can be found the smallest ΔT is still too large for Bi-2212 powders, which indicates that the composition homogeneity of Bi-2212 precursor powders needs to be improved further in the future.

What's more, the morphology of the precursor powders is showed in Fig. 5. It can be found Bi-2212 crystals were basically flakes, and the planar size was much larger than its thickness. In addition, the thickness information in detail was magnified on the right side of Fig. 5. It can be discovered that along the thickness direction, one Bi-2212 particle was commonly stacked and composed of several flakes. Then based on these pictures, $S_{\text{in-plane}}$ and the planar size distribution for Bi-2212 crystals were analyzed from ~200 crystals respectively for each precursor powder. From Fig. 6, it is found the planar size was basically in the range of 0 to 6 μm. The total frequency for the planar size located between 0.5 and 2.0 μm was basically larger than 70% except SP-Bi2.07–1. For SP-Bi2.07–2, its planar size located between 0.5 and 2.0 μm was the largest to be 89%.

However, for SP-Bi2.07–1, the planar size which occupied more than 70% was mainly located between 1.0 and 2.5 μm. Finally, $S_{\text{in-plane}}$ was calculated to be 1.26 ± 0.75 μm, 1.60 ± 0.66 μm, 2.03 ± 0.79 μm, and 1.38 ± 0.53 μm for CP-Bi2.17, SP-Bi2.17, SP-Bi2.07–1, and SP-Bi2.07–2 respectively. Most of the time Bi-2212 flakes lay on the planar directions in SEM view. Therefore, the crystal number used for the thickness analysis was much smaller. Here, $S_{\text{in-thickness}}$ was averaged from ~10 crystals and provided here for a rough reference. $S_{\text{in-thickness}}$ was 53 nm, 81 nm, 71 nm, and 187 nm for CP-Bi2.17, SP-Bi2.17, SP-Bi2.07–1, and SP-Bi2.07–2 respectively.

It is then found both the planar and the thickness size obtained from SEM images were basically consistent with that evaluated from FWHM value for these powders except the thickness size for SP-Bi2.17 and SP-Bi2.07–2. For FWHM value indicated that the thickness of SP-Bi2.17 was only a little smaller than that of SP-Bi2.07–2, while the statistical data found that the thickness of SP-Bi2.17 was much smaller than that of SP-Bi2.07–2. This might be mainly ascribed to the too small sample capacity analyzed for the thickness. Then combining with the preparation process for the precursor powders, it is then deduced that both the lowest planar and thickness size of CP-Bi2.17 might result from the mechanical grinding in its whole preparation process. This was easy to be understood for the grinding process will break Bi-2212 flakes from both the planar and the thickness direction. And the mechanical grinding was thought to be much more violent than the manual grinding. Moreover, it seemed that the thickness size and the planar size varied in a reverse direction for the precursor powders synthesized by SP. It can be explained by the competitive growth in these two vertical directions. This phenomenon had been reported and explained in our previous article [16]. However, the reason of how the size

Fig. 5 The morphology for the precursor powders (left) and the magnification of the red circles in the left images (right): **a** and **b** CP-Bi2.17; **c** and **d** SP-Bi2.17; **e** and **f** SP-Bi2.07–1; **g** and **h** SP-Bi2.07–2 (the red arrows mean the total length of the labelled crystals)
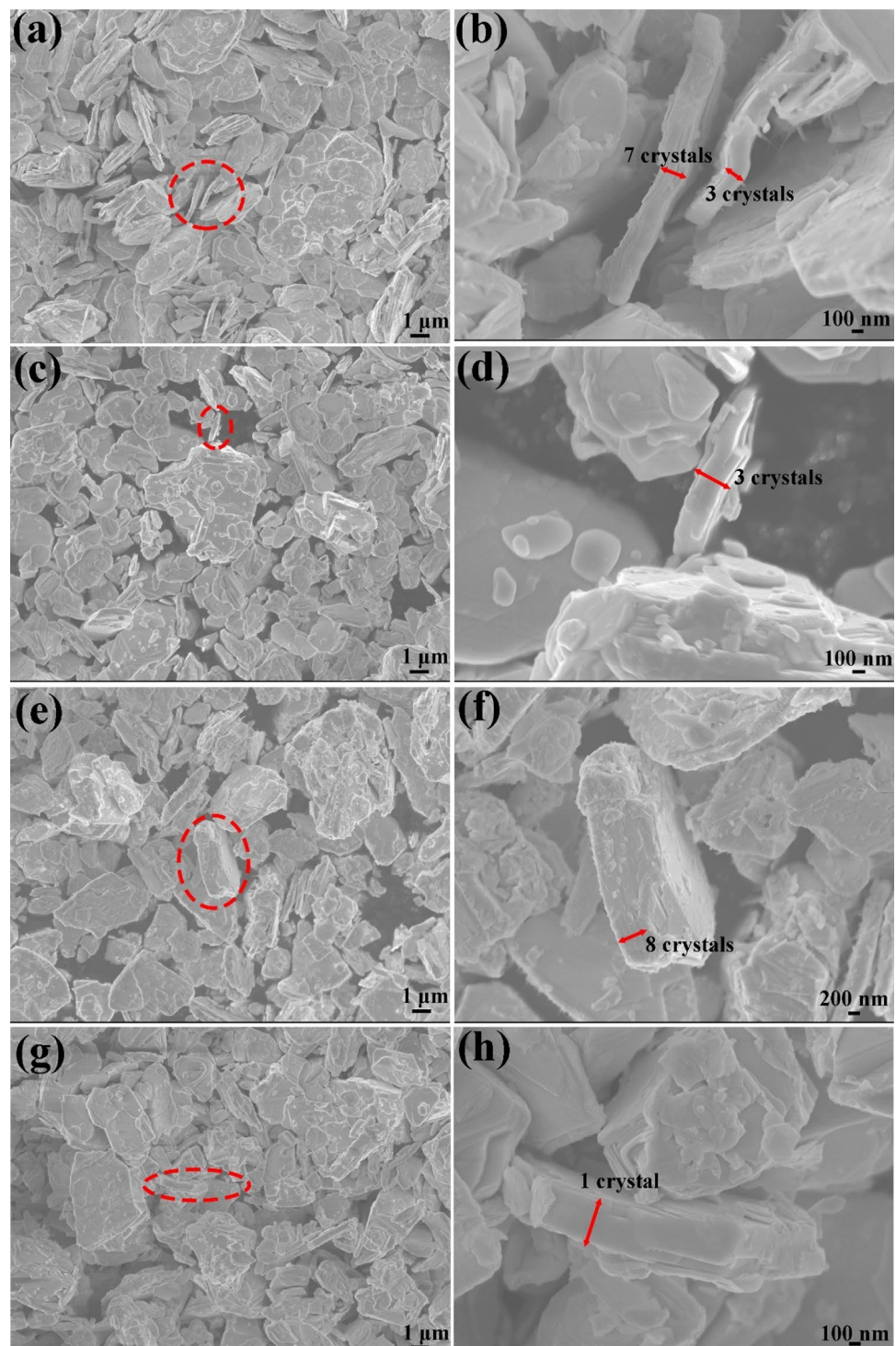
varied among the three powders was still unclear now. It is guessed that it might relate to the subtle elemental ratio variation or there might be another unknown factor controlling the growth of Bi-2212 crystals. In the future, the mechanism controlling the growth of Bi-2212 crystals needs to be studied deeply.

In Fig. 7, both SEM and BSE images taken at the same place were put together to check the existence of the second phase. It is discovered that no second phase was found in all the precursor powders, which was basically consistent with XRD results above except SP-Bi2.17. It is deduced that both the small content and the small size of
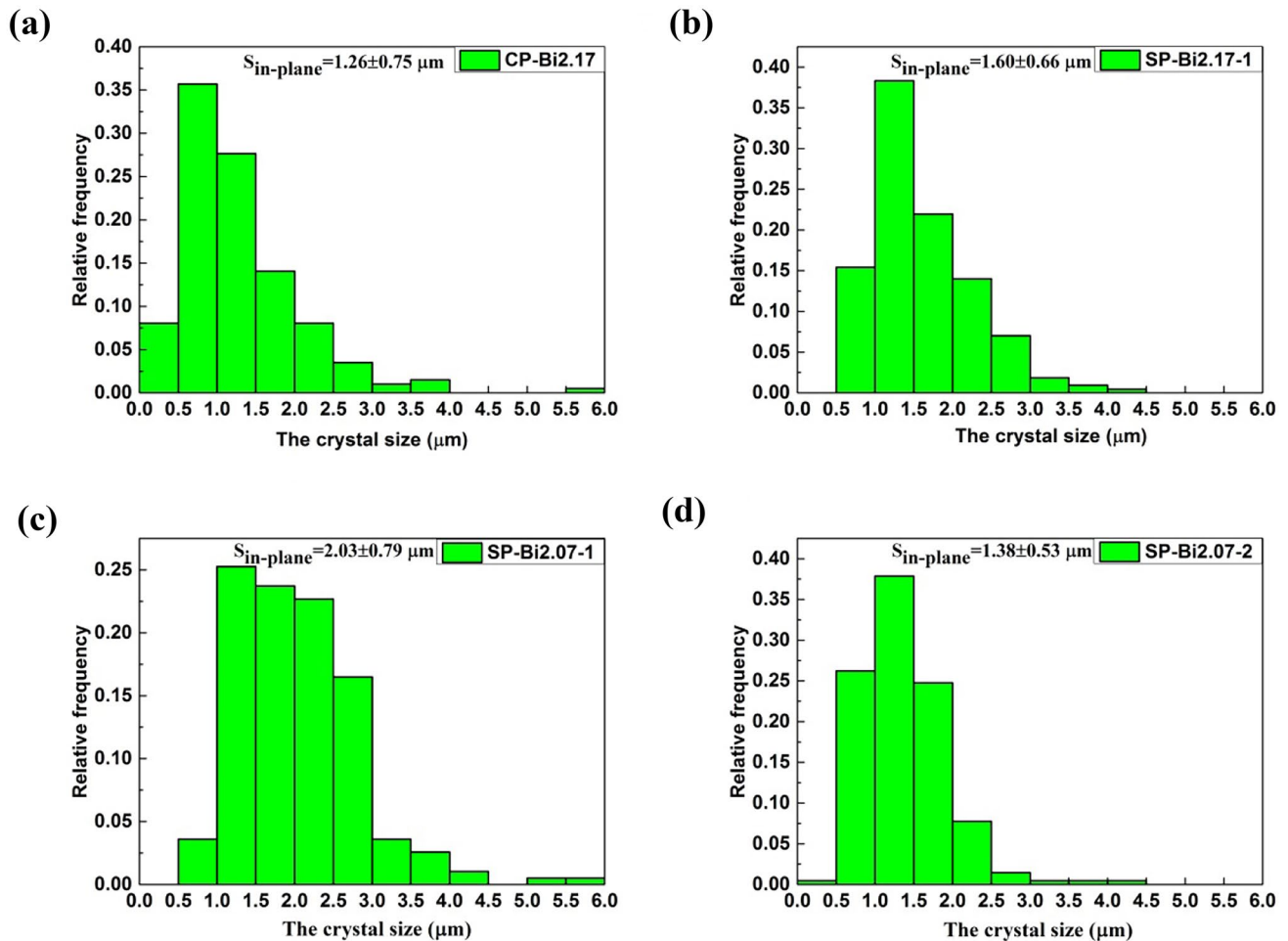
(a)

(b)

(c)

(d)

Fig. 6 The average planar size and the planar size distribution for Bi-2212 crystals in the precursor powder of **a** CP-Bi2.17, **b** SP-Bi2.17, **c** SP-Bi2.07–1, and **d** SP-Bi2.07–2

Bi-2201 in SP-Bi2.17 resulted in its difficult detection in BSE. In addition, from these BSE images, quite blur and local color inhomogeneity were observed in CP-Bi2.17, while the color distribution was much more homogeneous for the other three powders prepared by SP. This might indicate again that the composition homogeneity of powders synthesized from SP was better than that synthesized from CP.

3.2 The Machinability of the Wires

Figure 8 showed the transverse cross-section for the four machined wires. The basic information including D_a, R_a, and f are analyzed and listed in Table 3.

From Table 3, it is found D_a showed no obvious difference among the four wires. R_a was the smallest for W-CP-Bi2.17. R_a of W-CP-Bi2.07–2 was located at the

second place. And R_a of the other two wires was basically the same and also the largest. The smaller R_a always meant the shape of the filaments was closer to the round shape. And R_a data was thought to relate to the different machinability of the wires. Considering all the machining processes were kept exactly the same for these wires, R_a was deduced to be mainly influenced by the different feature of the precursor powder. Combined with the microstructure characterization results for the precursor powders, it is suspected that the planar size of the precursor powders might affect the machinability of the wires a lot. In the initial machining process, the powder slides easily in the first Ag tube, while the powder will be densified gradually later. At the final stage of the machining, the harness of the densified powder might become larger than that of Ag matrix. D_a was the same; therefore, wires prepared by the precursor powder with a larger planar size

Fig. 7 SEM and BSE images taken at the same place for the squeezed precursor powders **a** and **b** CP-Bi2.17; **c** and **d** SP-Bi2.17; **e** and **f** SP-Bi2.07–1; **g** and **h** SP-Bi2.07–2
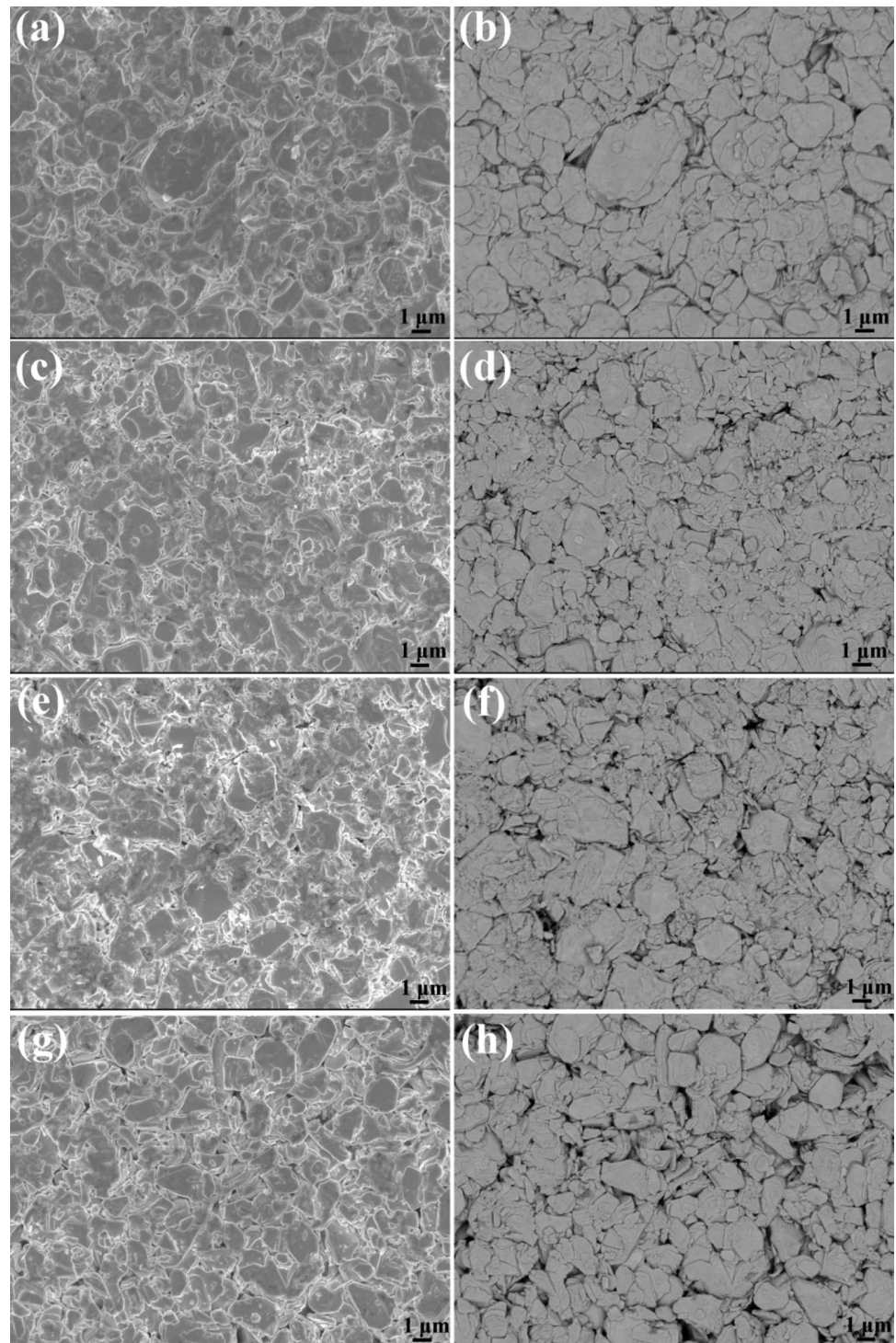
might have more probability to slide through Ag matrix and lead to the less regular shape of the filaments. And it just turned out the smaller planar size of the precursor powders basically corresponded to the smaller R_a of the machined wires. Therefore, it is deduced that decreasing the planar size of Bi-2212 crystals in the precursor powder might be beneficial to improve the machining homogeneity and result in a smaller R_a.
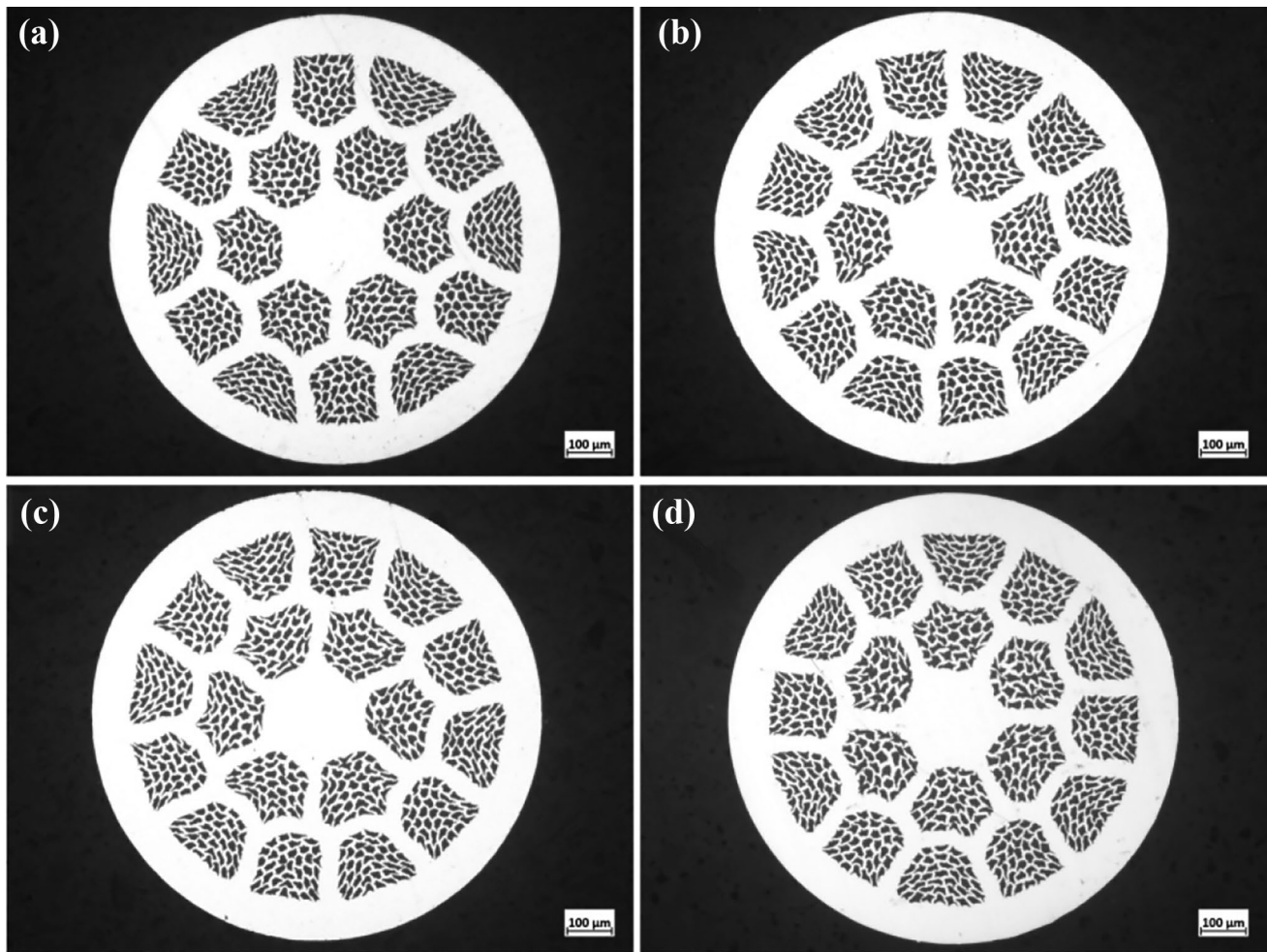
Fig. 8 The transverse cross-section for the four machined wires

3.3 The Processing Window and Current-Carrying Property of the Wires

3.3.1 The Processing Window and Current-Carrying Property of Bi-2212 Wires

Figure 9a shows the variation of J_e with T_{max}. T_p are then obtained and listed in Table 4. At the same time, the temperature accuracy of the furnace (T_a) for retaining $90\%*J_{e\text{-max}}$ of the wires is also presented in Table 4. From Table 4, it can be found T_a was smallest for W-CP-Bi2.17 and it was

larger for W-SP-Bi2.07–1 and W-SP-Bi2.07–2. A smaller T_a meant a higher requirement of the temperature accuracy for the furnace, which will increase the application cost of Bi-2212 wires. Correspondingly, the requirement for T_a was the largest for W-CP-Bi2.17 and smallest for W-SP-Bi2.07–1 and W-SP-Bi2.07–2 to retain their $90\%*J_{e\text{-max}}$. Figure 9b shows the maximum J_c ($J_{c\text{-max}}$) for the four wires. $J_{c\text{-max}}$ was the smallest for W-SP-Bi2.17, and $J_{c\text{-max}}$ of W-CP-Bi2.17 was larger. $J_{c\text{-max}}$ for W-SP-Bi2.07–1 and W-SP-Bi2.07–2 was basically the same with each other and was also the largest among these wires.

3.3.2 The Microstructure and Phase Composition of Bi-2212 Wires

Figure 10 shows the macrostructure of the four annealed wires holding the highest J_e. The coupling of the filaments can be observed clearly, which was always a key factor to influence the whole texture of Bi-2212 wires [21, 22]. The filaments' coupling in W-CP-Bi2.17 seemed to be the least

Table 3 The basic information for the four machined wires

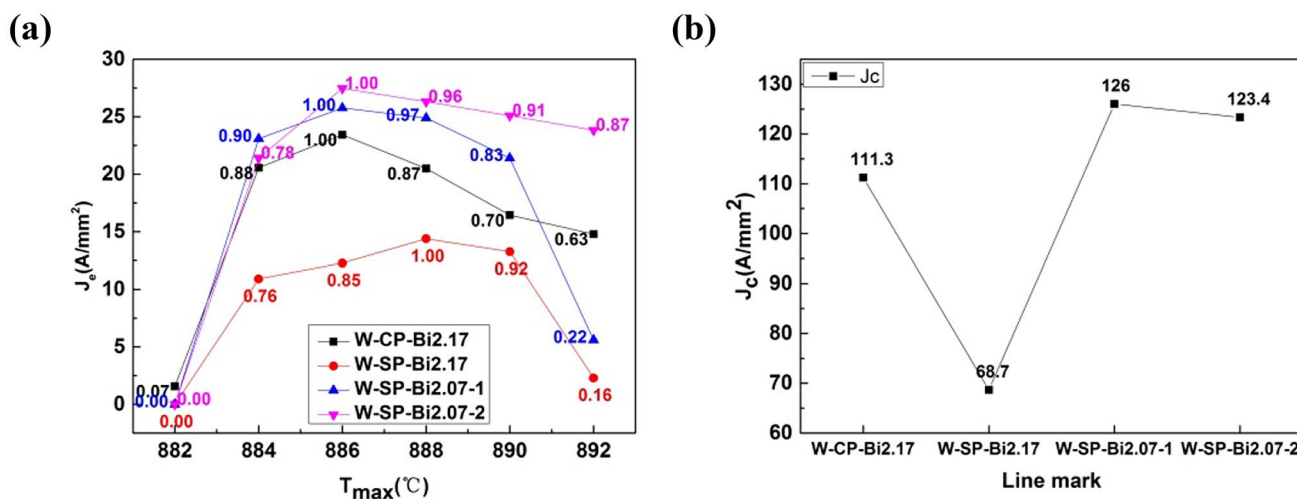| Line mark	D_a (μm)	R_a	f
W-CP-Bi2.17	18.04 ± 2.29	1.66 ± 0.46	21.07%
W-SP-Bi2.17	18.14 ± 2.20	1.83 ± 0.91	20.95%
W-SP-Bi2.07–1	17.84 ± 1.91	1.83 ± 0.55	20.45%
W-SP-Bi2.07–2	18.89 ± 3.28	1.79 ± 0.62	22.27%

(a)

(b)

Fig. 9 **a** The variation of J_e with T_{max}. **b** The maximum J_c for the four wires

because of the minimum connected branches of Bi-2212 crystals between their neighboring filaments. The coupling of the filaments in W-SP-Bi2.07–2 became larger, and that was the most severe in both W-SP-Bi2.17 and W-SP-Bi2.07–1. This result was consistent with R_a value obtained above. With the same D_a, the larger R_a corresponded to the more severe coupling of the filaments. It is easy to be understood because the less round filaments had more probability to be connected with its neighboring filaments, resulting in a higher probability of coupling.

Figure 11 showed the microstructure taken under BSE pattern for both the transverse and the longitudinal cross-sections for the four wires holding the highest J_e. Bi-2201 and 1:2 AEC were the second phases mostly observed in all the wires. The coupling states of the filaments were also consistent with that observed in Fig. 10. In addition, the area of Bi-2201 phase was found to be largest obviously in W-SP-Bi2.17 observed from both the transverse and the longitudinal cross-sections.

To learn more about the microstructure detail of the four wires, one side of transverse cross-section of the wires holding J_{e-max} was mirror-polished according to the methods elaborated in 2.2. Then, the polished wires were sintered under 0.1 MPa O_2 at 800 °C for 1 h, which were further observed under BSE pattern (Fig. 12) to check the texture and connectivity detail. Here it should be noticed that this

Table 4 T_p and the corresponding T_a for the four wires

Line mark	T_p (°C)	T_a (°C)
W-CP-Bi2.17	886	± 1
W-SP-Bi2.17	888–890	± 2
W-SP-Bi2.07–1	884–888	± 3
W-SP-Bi2.07–2	886–890	± 3

method of post-annealing samples at a temperature lower than the highest sintering temperature of the samples was a common way used in ceramic samples. This can bare the grain boundaries of samples and provide more detail information for the samples. And the premise is that there is no phase variation during the post-annealing. From both Hao's [23] and Matras's articles [24], it is deduced that no phase variation or quite limited phase variation existed in Bi-2212 wires sintered under 820 °C for a short period. From Fig. 12, lots of small light-gray phases marked by the yellow round circles were found everywhere, which was confirmed by EDS to be the mixture of Sr and O elements (Sr_xO_y). The reason for the existence of Sr_xO_y was not clear now, which needs further study in the future. However, the content of Bi-2201 was still the largest in W-SP-Bi2.17, while that in the other three samples was much smaller. And this was consistent with that observed in Fig. 11. Though the microstructure in Fig. 12 was definitely not the real microstructure of Bi-2212 crystals in the annealed Bi-2212 wires because of their extra sintering step at 800 °C, it is thought this microstructure can still reflect lots of detail information for the Bi-2212 crystals in the annealed Bi-2212 wires.

From Fig. 12, the assembling and interior texture information for Bi-2212 crystals can be clearly observed for the first time. There are much more different orientations of Bi-2212 crystals in W-CP-Bi2.17, which indicated the number of the nucleation cores in Bi-2212 phase during the cooling stage of the sintering process was much larger. The assembling and texture of Bi-2212 crystals were better in W-CP-Bi2.07–1 and best in W-CP-Bi2.07–2. It is then discovered that the assembling of Bi-2212 crystals in these wires seemed to be closely related to their ΔT. A higher ΔT was deduced to bring much more nucleation cores under the same cooling rate because of the worse composition
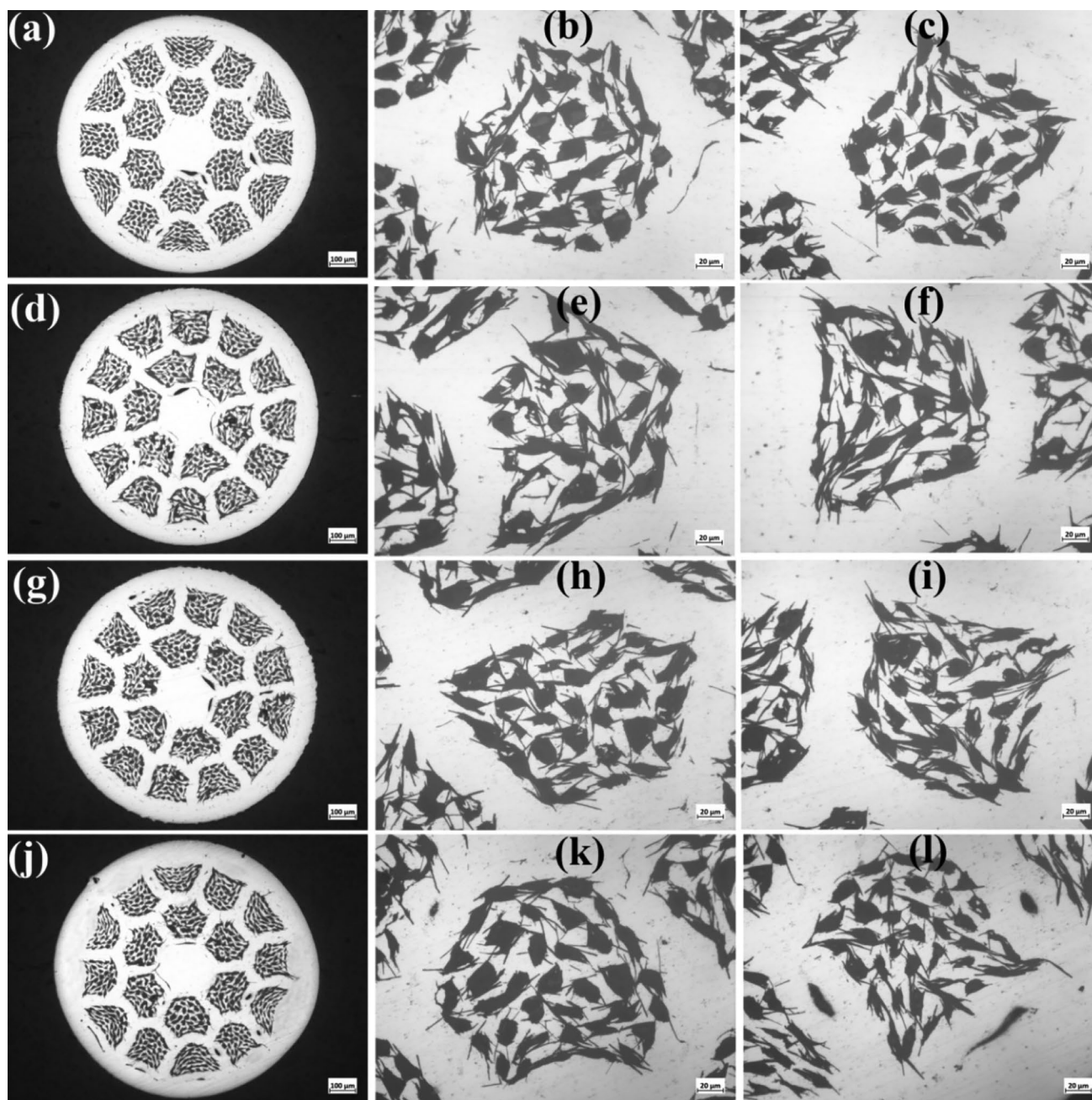
Fig. 10 The transverse cross-section for the four annealed wires holding the highest J_e **a, b, c** W-CP-Bi2.17; **d, e, f** W-SP-Bi2.17; **g, h, i** W-SP-Bi2.07–1; **j, k, l** W-SP-Bi2.07–2 (the center column is a representative area from the inner ring and the right column area from the outer ring)

homogeneity. And more nucleation cores will then lead to the worse assembling of Bi-2212 crystals. What's more, it can be found the assembling of Bi-2212 crystals differentiated with each other a lot even in the same wires, which was obvious especially in W-CP-Bi2.17. This might also result from its highest ΔT and verify its worst composition homogeneity. The better assembling of Bi-2212 crystals in W-CP-Bi2.07–2 compared with that in W-CP-Bi2.07–1 was thought to be related to the higher thickness of Bi-2212

crystals in the precursor powder. With the same ΔT, the higher thickness of Bi-2212 crystal itself might be beneficial to the assembling of Bi-2212 crystals in the sintering process and improve its texture in the interior of the filaments.

In addition, the connectivity between Bi-2212 crystals might also be reflected from Fig. 12. There are lots of quite small gaps that appeared at the boundaries of Bi-2212 crystal clusters. The gaps existing in the single Bi-2212 phase were thought to mainly result from the following two

Fig. 11 The microstructure observed on the transverse (left) and the longitudinal (right) cross-sections for the four wires holding the highest J_e: **a, b** W-CP-Bi2.17; **c, d** W-SP-Bi2.17; **e, f** W-SP-Bi2.07–1; **g, h** W-SP-Bi2.07–2
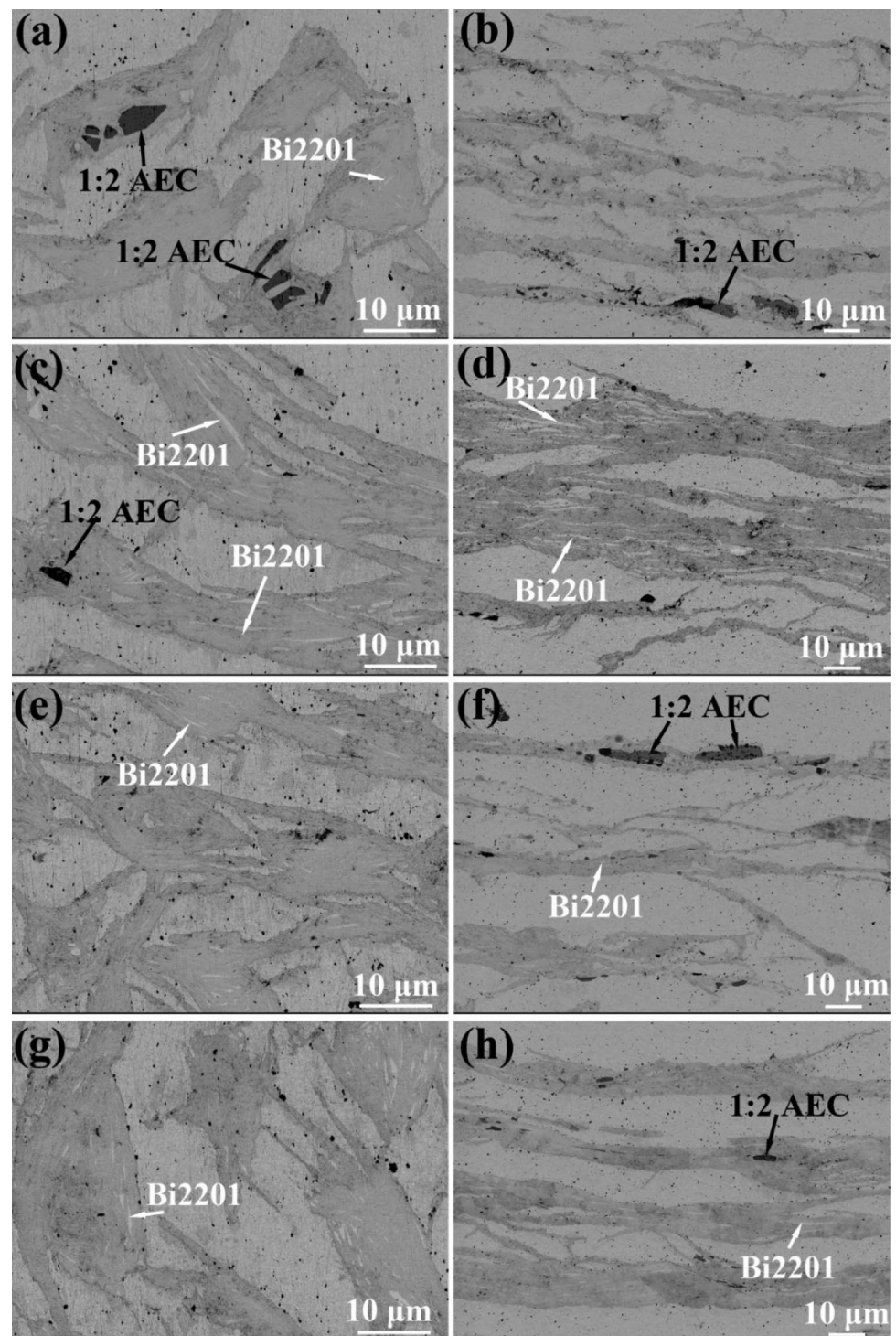
reasons. One is the anisotropy of the thermal expansion coefficient in Bi-2212 itself [25–27], which will lead to the gaps appearing at the high -angle boundaries between Bi-2212 crystal clusters. The second reason might also relate to the composition inhomogeneity of the powder, which will also cause the subtle difference of the thermal expansion coefficient. Therefore, both the more consistent assembling of Bi-2212 crystals and the better composition homogeneity of Bi-2212 precursor powders meant both the smaller number and the narrower distance of gaps. Then, it is deduced that these gaps appearing here may reflect both the connectivity and composition homogeneity of Bi-2212 crystals. And the connectivity in W-SP-Bi2.07–2 might be best while that in W-CP-Bi2.17 was worst.

Fig. 12 The transverse cross-section taken under BSE pattern for the annealed Bi-2212 wires holding $J_{\text{e-max}}$ sintered further at 800 °C for 1 h under O_2: **a** and **b** W-CP-Bi2.17; **c** and **d** W-SP-Bi2.17; **e** and **f** W-SP-Bi2.07–1; **g** and **h** W-SP-Bi2.07–2
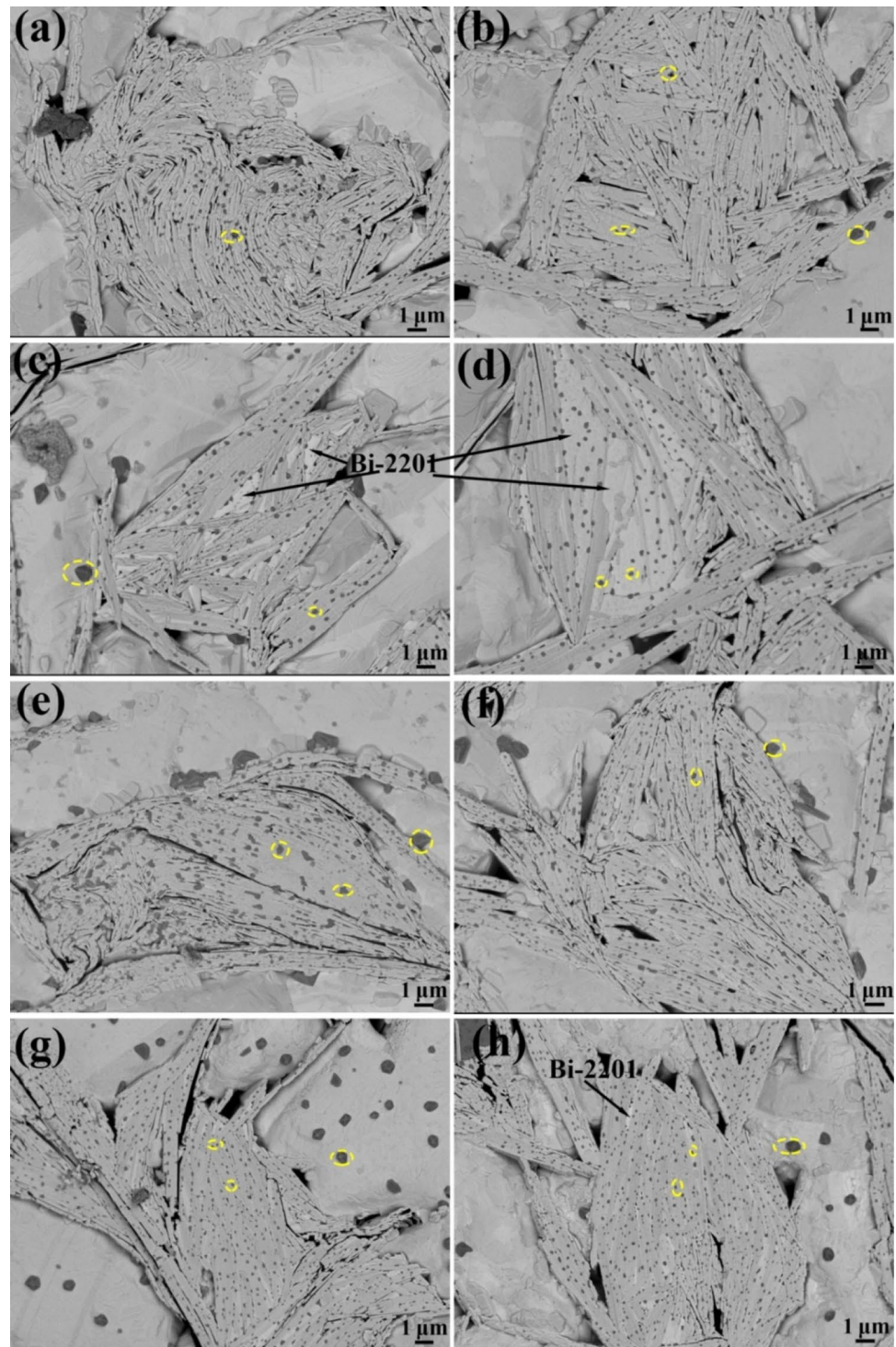
What's more, the connectivity of Bi-2212 crystals seemed to be also closely related to the assembling or the interior texture of Bi-2212 filaments. From Fig. 12, it can be found both the number and the distance of gaps were smaller in the wires with better assembling of Bi-2212 crystals. In theory, the Bi-2212 crystals assembled in a more consistent direction, and both the decreased high angle boundaries and the decreased gaps will enhance its connectivity because of the much more consistent thermal expansion coefficient. Therefore, the better texture of Bi-2212 crystals in the interior of Bi-2212 filaments might correspond to the better connectivity of Bi-2212 crystals. The connectivity of Bi-2212 crystals was always thought to be quite an important factor influencing J_c. Eliminating
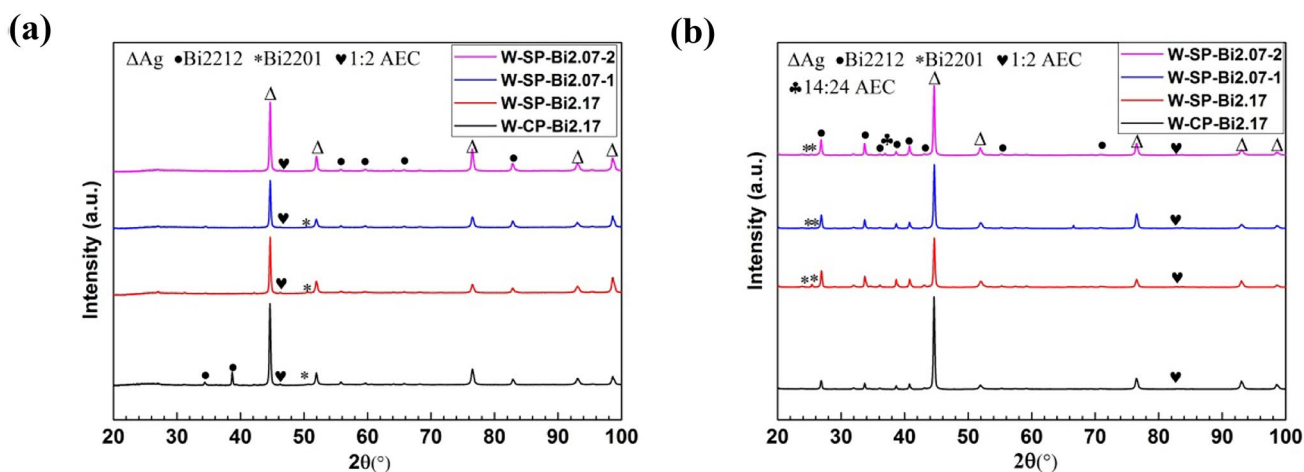
Fig. 13 The micro-area XRD detected **a** on the transverse cross-section and **b** on the longitudinal cross-section for the four wires

the porosity on the macrostructure of Bi-2212 wires was a key way to enhance the connectivity of Bi-2212 crystals. However, the methods to improve the connectivity on the microstructure seemed to be not mentioned until now. The highest J_c recorded for Bi-2212 wires was reported to be related to the improved connectivity in its wire [17]. And this wire was latterly also confirmed to hold the quite high texture [18]. Both W-SP-Bi2.07–1 and W-SP-Bi2.07–2 holding the highest J_c in this article were also proved to have the best connectivity and the highest texture in the interior of Bi-2212 filaments observed from Fig. 12.

The corresponding micro-XRD data for the four wires holding the highest J_e were plotted in Fig. 13. Some more detailed analyses based on Fig. 13 are listed in Tables 5, 6, 7, and 8 for comparison convenience.

By analyzing all the data obtained from the micro-area XRD showed above, some certain conclusions can be obtained. Firstly, Bi-2201 and 1:2 AEC were also confirmed to be the main second phases, which was consistent with EDS data above. The much larger content of Bi-2201 in W-SP-Bi2.17 detected on both the transverse and longitudinal cross-sections was also consistent with the results obtained above. It also indicated there was ~5.95% 1:2 AEC phase existing in W-SP-Bi2.17 on the transverse cross-section, while its content became quite small on the longitudinal cross-section. The existence of 1:2 AEC had been checked by EDS, and

here its quantitative content was provided for the four wires from the micro-area XRD. The inconsistence content of 1:2 AEC on the two directions might be mainly ascribed to the large difference of the tested area. For in the micro-XRD test, the number of filaments detected on the transverse cross-section was much larger than that detected on the longitudinal cross-section. In addition, ~3% 1:2 AEC was both discovered in W-CP-Bi2.17 on its transverse-cross section and in W-SP-Bi2.07–2 on its longitudinal cross-section. The largest content of Bi-2201 in W-SP-Bi2.17 was mainly ascribed to the extra Bi-2201 found in its precursor powder. As for the reason of the appearance of 1:2 AEC and its content variation, it needs further study in the future. Secondly, both the texture and the crystal size of Ag matrix did not have an obvious difference among the four wires. This indicated that Ag matrix will not be a main factor to affect both the microstructure and J_c of the four wires. Thirdly, the texture of Bi-2212 phase both on the transverse and longitudinal cross-sections for W-CP-Bi2.17 and W-SP-Bi2.07–2 was larger compared with the other two wires. And the texture of Bi-2212 phase for W-SP-Bi2.07–2 was better compared with that for W-CP-Bi2.17. As for the texture variation of these wires, it will be explained in detail in the fourth part of 3.3.

Figure 14a provided the AC susceptibility for W-CP-Bi2.17, W-SP-Bi2.07–1, and W-SP-Bi2.07–2 tested under 0.1 Oe from 4.2 to 105 K. The lowest J_c of W-SP-Bi2.17

Table 5 The information of Ag and Bi-2212 phases analyzed based on the micro-area XRD detected on the transverse cross-section for the four wires

Sample	(111) of Ag		$T_{Ag\text{-}PI}$	$T_{Ag\text{-}PA}$	(040) of Bi-2212		$T_{CS\text{-}PI}$	$T_{CS\text{-}PA}$
	2θ	FWHM			2θ	FWHM		
W-CP-Bi2.17	44.64	0.251	73.10%	64.31%	82.93	0.425	57.30%	60.02%
W-SP-Bi2.17	44.67	0.243	73.85%	64.20%	82.89	0.464	36.49%	46.59%
W-SP-Bi2.07–1	44.67	0.253	72.17%	62.65%	82.93	0.455	39.68%	54.60%
W-SP-Bi2.07–2	44.65	0.253	65.59%	58.98%	82.84	0.418	51.61%	60.04%

Table 6 The information of Bi-2201 and AEC phases analyzed based on the micro-area XRD detected on the transverse cross-section for the four wires

Sample	(315(-)) of Bi-2201		$M_{Bi\text{-}2201\text{-}PI}$	$M_{Bi\text{-}2201\text{-}PA}$	(406) of 1:2 AEC		$M_{ACE\text{-}PI}$	$M_{AEC\text{-}PA}$
	2θ	FWHM			2θ	FWHM		
W-CP-Bi2.17	50.62	0.1	1.90%	0.12%	46.299	0.216	3.29%	2.81%
W-SP-Bi2.17	50.62	0.1	10.49%	4.14%	46.289	0.229	6.74%	5.16%
W-SP-Bi2.07–1	50.64	0.1	1.89%	0.10%	46.19	0.1	2.65%	0.14%
W-SP-Bi2.07–2	-	-	0.00%	0.00%	46.18	0.1	2.36%	0.11%

was thought to be mainly resulted from its largest content of the second phases, whose AC susceptibility was not tested here. The AC susceptibility is an effective method to obtain T_c and characterize the inter-grain connectivity of the superconducting crystal. There are mainly two obvious drops for χ' with temperature decreased. The first drop can be recognized as T_c for the samples, which can be obtained by extrapolating the high-temperature part of the curve to the zero magnetization. The other drop of χ' presented the coupling signal, which was caused by the macroscopic shielding currents by the grains and the grain boundaries [28]. A peak also appeared in the imaginary part of the AC susceptibility, which can reflect the dissipation mechanism due to the vortex motion [29]. Here, the dissipation peak position of χ'' was defined as T_{peak}. According to Kim's study [30], the shifting of T_{peak} to the lower temperature suggested the weaker superconducting coupling across the grain boundaries. Then T_c and T_{peak} for the three wires were obtained and plotted in Fig. 14b. It can be seen that T_c and T_{peak} varied in the same trend among the three wires. T_c and T_{peak} were both highest in W-SP-Bi2.07–2, indicating its best oxygen doping state and the best connectivity of Bi-2212 crystals at the same time. T_c and T_{peak} were lowest in W-CP-Bi2.17. Here T_c was thought to be mainly related to the different oxygen doping level in these wires, which was mainly decided by the original oxygen level in the precursor powder considering the same sintering process for these wires. As for T_{peak}, it is found the data was exactly consistent with the connectivity state discovered above. T_{peak} was the highest for W-SP-Bi2.07–2 holding the best connectivity and it was the lowest for W-CP-Bi2.17 holding the worst connectivity. This also verified that the provided method in 2.2 was quite effective to characterize the connectivity of Bi-2212 crystals.

3.3.3 The Influence of the Precursor Powder on T_p of Bi-2212 Wires

From Table 3, it can be found T_p was smallest for W-CP-Bi2.17 and largest for W-SP-Bi2.07–1 and W-SP-Bi2.07–2. Combing with the corresponding ΔT value, it is found the higher ΔT seemed to correspond to the smaller T_p. The lower ΔT value for the precursor powders obtained from SP indicated that SP had the advantages of preparing the precursor powder with the higher composition homogeneity. In addition, it is found the second phases like Bi-22201 might also contribute to the increase of ΔT.

The larger ΔT of Bi-2212 precursor powder influenced the nucleation behavior of Bi-2212 crystals a lot in the sintering process, which eventually led to both the worse texture and weaker connectivity of Bi-2212 crystals in the interior of Bi-2212 filaments. The slow cooling rate in the sintering process for Bi-2212 wires contributed a lot to the high texture formed later [31]. Though the solidification and nucleation mechanisms of Bi-2212 phases in the partial melting process were not exactly clear now, the increased nucleation cores resulting from the worse composition homogeneity were definitely detrimental to both the assembling and connectivity of Bi-2212 crystals under the same cooling process. Eventually the larger ΔT brought the larger perturbation to I_c by deteriorating both the interior texture and the connectivity of Bi-2212 crystals to a larger extent. What's more, the higher ΔT of the precursor powder led to the melting of Bi-2212 crystal less completely compared with the precursor powder holding a lower ΔT under the same T_{max}. The precursor powder holding the higher ΔT finally resulted in the melting of Bi-2212 crystals that happened in a larger temperature scale and led to a smaller T_p.

Table 7 The information of Ag and Bi-2212 phases analyzed based on the micro-area XRD detected on the longitudinal cross-section for the four wires

Sample	(111) of Ag		$T_{Ag\text{-}PI}$	$T_{Ag\text{-}PA}$	(008) of Bi-2212		$T_{LS\text{-}PI}$	$T_{LS\text{-}PA}$
	2θ	FWHM			2θ	FWHM		
W-CP-Bi2.17	44.62	0.260	81.24%	72.21%	26.87	0.279	71.93%	72.85%
W-SP-Bi2.17	44.65	0.272	72.41%	60.77%	26.93	0.268	66.84%	62.06%
W-SP-Bi2.07–1	44.67	0.269	68.54%	68.53%	26.87	0.285	68.54%	68.53%
W-SP-Bi2.07–2	44.65	0.266	75.04%	65.71%	26.88	0.279	81.51%	82.47%

Table 8 The information of Bi-2201 and AEC phases analyzed based on the micro-area XRD detected on the longitudinal cross-section for the four wires

Sample	(006) of Bi-2201		$M_{Bi-2201-PI}$	$M_{Bi-2201-PA}$	(755) of 1:2 AEC		M_{AEC-PI}	M_{AEC-PA}
	2θ	FWHM			2θ	FWHM		
W-CP-Bi2.17	-	-	0.00%	2.81%	83.740	0.1	0.79%	0.05%
W-SP-Bi2.17	25.430	0.210	6.17%	5.16%	83.798	0.412	0.57%	0.79%
W-SP-Bi2.07–1	23.359	0.203	2.96%	0.14%	83.740	0.379	1.17%	1.62%
W-SP-Bi2.07–2	25.321	0.235	2.81%	0.11%	83.759	0.345	3.64%	2.94%

Therefore, increasing the composition homogeneity of Bi-2212 phase itself and decreasing the content of the impurity phases existing in Bi-2212 precursor powder might be the key methods to control the melting behavior of Bi-2212 crystals and to improve T_p of Bi-2212 wires. SP had been proved to be a better method to prepare the precursor powder with a smaller ΔT. In the future, factors influencing ΔT of the precursor powder prepared by SP need to be studied further to decrease its ΔT.

### 3.3.4 The Influence of the Precursor Powder on J_c of Bi-2212 Wires

Factors influencing J_c of Bi-2212 wires are quite complicated, mainly including the type and content of the second phase, the texture of Bi-2212 crystals, T_c, and the connectivity of Bi-2212 crystals. Both the largest content of Bi-2201 and 1:2 AEC had been found in W-SP-Bi2.17. The existence of Bi-2201 in SP-Bi2.17 should take responsibility for its largest content of second phases in W-SP-Bi2.17. Three percent 1:2 AEC phase was both found in W-CP-Bi2.17 and W-SP-Bi2.07–2. And the phase purity was the highest in W-SP-Bi2.07–1.

As for the texture of Bi-2212 wires, it is discovered that both the interior texture of the filaments and the coupling of the neighboring filaments contributed to its final texture. Though the interior texture of Bi-2212 filaments seemed to be worst in W-CP-Bi2.17, its smallest coupling between the neighboring filaments finally made its texture rank secondly in the four wires. Combining with the best interior texture in Bi-2212 filaments and a subtle coupling between the neighboring filaments, W-SP-Bi2.07–2 entailed the best texture finally. Though the interior texture was good for W-SP-Bi2.07–1, its most severe coupling led to its final texture ranked thirdly among the four wires. And W-SP-Bi2.17 held the worst texture because of both its most severe coupling and bad interior texture of Bi-2212 filaments.

As for the connectivity of Bi-2212 crystals, it had been found the connectivity of Bi-2212 crystals has a close relation with its interior texture. Better texture in the interior of Bi-2212 filaments had been proved to correspond to a better connectivity of Bi-2212 crystals. And the connectivity state was also verified by T_{peak} data obtained from the AC susceptibility. Therefore, the connectivity of Bi-2212 crystals was best in W-SP-Bi2.07–2 and worst in W-CP-Bi2.17. And the connectivity of Bi-2212 crystals in W-SP-Bi2.07–1 ranked secondly.

Eventually, the largest content of the second phases in W-SP-Bi2.17 was the main reason leading to its lowest J_c among the four wires. It should be noticed here that J_c of
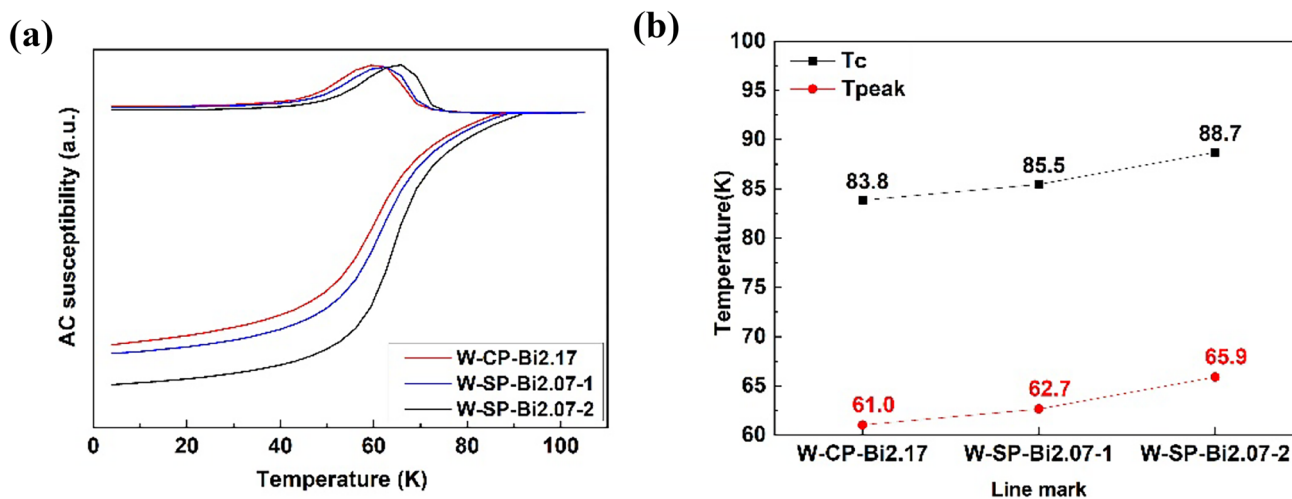
Fig. 14 a AC susceptibility tested under 0.1 Oe from 4.2 to 105 K. **b** T_c and T_{peak} for the four wires

W-SP-Bi2.17 was much lower compared with the other three wires, which indicated the large content of the second phases deteriorates J_c a lot. W-SP-Bi2.07–1 held the highest phase purity, while its T_c was just a little smaller and its connectivity and texture were just a little worse than those of W-SP-Bi2.07–2. Therefore, eventually J_c of W-SP-Bi2.07–1 and W-SP-Bi2.07–2 was basically the same with each other and was also the highest in the four wires. The total texture for W-CP-Bi2.17 ranked secondly in the four wires; however, it still had ~3% content of 1:2 AEC, and its lowest T_c and the worst connectivity made its J_c rank thirdly in these wires.

4 Conclusions

All in all, the feature of the four precursor powders, the microstructure, and property of the four wires made from these powders were characterized comprehensively. The microstructure, T_p, and J_c of these Bi-2212 wires were closely related to the feature of these precursor powders. The main conclusions were summarized as follows:

1. The smaller planar size of Bi-2212 crystal in the precursor powder might be beneficial to improve the machining homogeneity of Bi-2212 wires, which will further decrease the coupling of neighboring filaments and improve its texture in the sintering process;
2. The larger thickness of Bi-2212 crystals in the precursor powder might be beneficial to the assembling of Bi-2212 crystals. Increasing the thickness of Bi-2212 crystals might be another way to improve its interior texture;
3. The composition homogeneity of the precursor powder can be evaluated by its ΔT. The higher ΔT indicated the worse composition homogeneity. In addition, Bi-2201 phase existing in the precursor powder will also lead to the increase of ΔT;
4. Compared with CP, SP showed a higher preparation efficiency of Bi-2212 precursor powders and Bi-2212 precursor powders prepared by SP had better composition homogeneity;
5. A higher ΔT in Bi-2212 precursor powder will lead to a smaller T_p in Bi-2212 wires and will also decrease both the interior texture and connectivity of Bi-2212 filaments;
6. The final texture of Bi-2212 wires was decided both by its interior texture in the filaments and the coupling state of the neighboring filaments.

SP was a promising method to prepare Bi-2212 precursor powders with better property. Influence of the specific feature of the precursor powder on both the microstructure and property of Bi-2212 wires was discussed deeply for the first time. The smaller planar size and the larger thickness of Bi-2212 crystals were beneficial to improve the texture of Bi-2212 wires. And the lower ΔT in the precursor powder can increase T_p, the interior texture, and connectivity of Bi-2212 wires. In the future, factors influencing the feature of the precursor powder need to be deeply studied to control its microstructure and improve its composition homogeneity.

References

1. Larbalestier, D.C., Jiang, J., Trociewitz, U.P., Kametani, F., Scheuerlein, C., Dalban-Canassy, M., Matras, M., Chen, P., Craig, N.C., Lee, P.J., Hellstrom, E.E.: Isotropic round-wire multifilament cuprate superconductor for generation of magnetic fields above 30 T. Nat. Mater. **13**(4), 375–381 (2014)
2. Huang, S.Z., Qin, J.G., Zhu, Y.L., Li, J.G.: Development situation and quality control of CICC in the future fusion reactors. Cryo. & Supercond. **44**(6), 27–33 (2016)
3. Chen, P., Trociewitz, U.P., Lu, J., Bosque, E.S., Jiang, J., Hellstrom, E.E., Larbalestier, D.C.: Experimental study on potential heat treatment issues of large Bi-2212 coils. IEEE Trans. Appl. Supercond. **27**(4), 4601405 (2017)
4. Liu, H., Ma, H., Liu, F., Shi, Y., Qin, J., Wu, Y., Li, J., Lei, L.: Experimental study on Bi-2212 cable-in-conduit conductor. IEEE Trans. Appl. Supercond. **28**(4), 4802104 (2018)
5. Qin, J., Wu, Y., Li, J., Dai, C., Liu, F., Liu, H., Liu, P., Li, C., Hao, Q., Zhou, C., Liu, S.: Manufacture and test of Bi-2212 cable-in-conduit conductor. IEEE T. Appl. Supercon. **27**(4), 1–5 (2017)
6. Qin, J., Shi, Y., Wu, Y., Li, J., Wang, Q., He, Y., Dai, C., Liu, F., Liu, H., Mao, Z., Nijhuis, A., Zhou, C., Devred, A.: First AC loss test and analysis of a Bi2212 cable-in-conduit conductor for fusion application. Supercond. Sci. Technol. **31**(1), 015010 (2018)
7. Rong, J., Huang, X., Song, Y., Yang, H., Lu, K.: AC losses calculation of Bi-2212 cable-in-conduit conductor used in CFETR. Fusion. Eng. Des. **141**, 109–115 (2019)
8. Tian, Z.J., Wang, W.T., Huo, B.L., Liu, L., Yang, Y., Zhao, Y.: Effect of dilute Co^{3+} doping on structure and superconducting properties of GdBCO thin films. Cryo. & Supercond. **49**(7), 5–9 (2021)
9. Wang, M.J., Wang, W.T., Liu, L., Tian, Z.J., Zhao, Y.: The electromagnetic properties of YGdBCO coated conductors with periodic micro-holes arrays. J. Alloy. Compd. **877**, 160138 (2021)
10. Shen, T., Garcia Fajardo, L.: Superconducting accelerator magnets based on high-temperature superconducting Bi-2212 round wires. Instruments. **4**(2), 1–22 (2020)
11. Rochester, J., Myers, C., Sumption, M., Shen, T., Majoros, M., Collings, E.W.: The magnetization of Bi:2212 rutherford cables

for particle accelerator applications. IEEE Trans. Appl. Supercond. **31**(5), 1–5 (2021)

12. Shen, T., Jiang, J., Kametani, F., Trociewitz, U.P., Larbalestier, D.C., Hellstrom, E.E.: Heat treatment control of Ag–$Bi_2Sr_2CaCu_2O_x$ multifilamentary round wire: investigation of time in the melt. Supercond. Sci. Technol. **24**(11), 115009 (2011)

13. Shen, T., Li, P., Ye, L.: Heat treatment control of Bi-2212 coils: I. Unravelling the complex dependence of the critical current density of Bi-2212 wires on heat treatment. Cryogenics **89**, 95–101 (2018)

14. Jiang, J., Hossain, S.I., Oloye, T.A., Oz, Y., Barua, S., Cooper, J., Miller, E., Huang, Y., Parrell, J.A., Kametani, F., Trociewitz, U.P., Hellstrom, E.E., Larbalestier, D.C.: Effects of wire diameter and filament size on the processing window of Bi-2212 round wire. IEEE Trans. Appl. Supercond. **31**(5), 1–6 (2021)

15. Jiang, J., Francis, A., Alicea, R., Matras, M., Kametani, F., Trociewitz, U.P., Hellstrom, E.E., Larbalestier, D.C.: Effects of filament size on critical current density in overpressure processed Bi-2212 round wire. IEEE Trans. Appl. Supercond. **27**(4), 6400104 (2017)

16. Li, Z.B., Liu, G.Q., Jiao, G.F., Xu, X.Y., Hao, Q.B., Bai, L.F., Yao, K., Li, C.S.: Influence of the precursor powder composition on the microstructure and the critical current density of Bi2212 wires. J. Mater. Sci. -Mater. El. **33**(26), 21111–21126 (2022)

17. Jiang, J., Bradford, G., Hossain, S.I., Brown, M.D., Cooper, J., Miller, E., Huang, Y., Miao, H., Parrell, J.A., White, M., Hunt, A., Sengupta, S., Revur, R., Shen, T., Kametani, F., Trociewitz, U.P., Hellstrom, E.E., Larbalestier, D.C.: High-performance Bi-2212 round wires made with recent powders. IEEE T. Appl. Supercon. **29**(5), 6400405 (2019)

18. Oloye, T.A., Matras, M., Jiang, J., Hossain, S.I., Su, Y., Trociewitz, U.P., Hellstrom, E.E., Larbalestier, D.C., Kametani, F.: Correlation of critical current density to quasi-biaxial texture and grain boundary cleanliness in fully dense Bi-2212 wires. Supercond. Sci. Technol. **34**(3), 035018 (2021)

19. Liu, G.Q., Jin, L.H., Xu, X.Y., Jiao, G.F., Zheng, H.L., Hao, Q.B., Cui, L.J., Yu, Z.M., Li, C.S.: Comparison of intermediate phase evolution in Bi-2212 powders prepared by spray pyrolysis and co-precipitation methods for high performance wires. Rare. Metal. Mat. Eng. **1**, 92–97 (2022)

20. Zhang, Y., Johnson, S., Naderi, G., Chaubal, M., Hunt, A., Schwartz, J.: High critical current density $Bi_2Sr_2CaCu_2O_x$/Ag wire containing oxide precursor synthesized from nano-oxides. Supercond. Sci. Technol. **29**(9), 095012 (2016)

21. Matras, M.: Investigation of Ag-sheathed multi-filamentaral $Bi_2Sr_2CaCu_2O_{8-x}$ superconducting round wires processed with overpressure, for high field magnets. PhD Thesis 1–128 (2016)

22. Angrisani Armenio, A., Leveratto, A., de Marzi, G., Traverso, A., Bernini, C., Celentano, G., Malagoli, A.: Investigation of transport mechanisms induced by filament-coupling bridges-network in Bi-2212 wires. Supercond. Sci. Technol. **35**(3), 035002 (2022)

23. Hao, Q.B., Li, C.S., Xu, X.Y., Liu, G.Q., Jiao, G.F., Zheng, H.L., Zhang, S.N., Li, G.S., Zhang, C.P., Yu, Z.M., Bai, L.F., Feng, J.Q., Zhang, P.X.: Effect of pre-annealing on microstructure, mechanical properties and current-carrying properties of Bi-2212 wires. Fusion. Eng. Des. **156**, 111606 (2020)

24. Matras, M.R., Jiang, J., Larbalestier, D.C., Hellstrom, E.E.: Understanding the densification process of $Bi_2Sr_2CaCu_2O_x$ round wires with overpressure processing and its effect on critical current density. Supercond. Sci. Technol. **29**(10), 105005 (2016)

25. Meingast, C., Junod, A., Walker, E.: Superconducting fluctuations and uniaxial-pressure dependence of Tc of a $Bi_2Sr_2CaCu_2O_{8+x}$ single crystal from high-resolution thermal expansion. Physica C **272**, 106–114 (1996)

26. Babaeipour, M., Ross, D.K.: A determination of the variation in the lattice parameters of $Bi_2Sr_2CaCu_2O_{8+x}$ (Bi-2212) as a function of temperature and oxygen content. Physica C **425**(3–4), 130–134 (2005)

27. Tenbrink, J., Krauth, H.: Thermal expansion properties of Bi-2212 in Ag or an Ag-alloy matrix. Supercond. Sci. Technol. **7**, 754–758 (1994)

28. Zhang, S., Li, C., Hao, Q., Ma, X., Lu, T., Zhang, P.: Optimization of Bi-2212 high temperature superconductors by potassium substitution. Supercond. Sci. Technol. **28**(4), 1–10 (2015)

29. Ge, J., Gutierrez, J., Li, M., Zhang, J., Moshchalkov, V.V.: Vortex phase transition and isotropic flux dynamics in $K_{0.8}Fe_2Se_2$ single crystal lightly doped with Mn. Appl. Phys. Lett. **103**(5), 052602:1–5 (2013)

30. Kim, S.S., Srinivasan, T.T., Newnham, R.E.: Weak-link nature of ac susceptibility in the grain-oriented $YBa_2Cu_3O_7$ superconducting ceramics. Phys. Stat. Sol. **123**, 275–283 (1991)

31. Aksenova, T.D., Bratukhin, P.V., Shavkin, S.V., Melnikov, V.L., Antipova, E.V., Khlebova, N.E., Shikov, A.K.: Texture formation in $Bi_2Sr_2Ca_1Cu_2O_x$ Ag tapes prepared by partial melt process. Physica C **205**(3–4), 271–279 (1993)